PAPER

Monolithic supports based on biomorphic SiC for the catalytic combustion of hydrogen†

G. M. Arzac,*[a] J. Ramírez-Rico,[ab] A. Gutiérrez-Pardo,[ab] M. C. Jiménez de Haro,[a] D. Hufschmidt,[a] J. Martínez-Fernández[ab] and A. Fernández*[a]

Catalytic hydrogen combustion was studied with H_2/air mixtures in conditions that simulate the H_2 concentration of the exhaust gases from fuel cells (3–4% v/v H_2 in air). Pt-impregnated monoliths based on porous biomorphic SiC (bio-SiC) substrates were employed for the first time for this reaction. Capillary forces were exploited for the incipient impregnation of supports with H_2PtCl_6 solutions. Freeze drying permitted us to obtain a homogeneous distribution of the active phase reducing accumulation at the monolith's outer shell. The supports and catalysts were characterized from a structural and thermal point of view. Catalytic tests were performed in a homemade reactor fed with up to 1000 ml min^{-1} H_2/air mixtures and a diffusional regime (non-isothermal) was achieved in the selected conditions. Catalyst loading was tested in the range of 0.25–1.5 wt% Pt and 100% conversion was achieved in all cases. Temperatures were recorded at different points of the monoliths during the reaction showing anisotropic thermal behavior for selected bio-SiC substrates. These effects are of interest for heat management applications and were explained in correlation with thermal conductivity measurements performed on the supports. Pt-impregnated monoliths were also tested in less than 100% conversion conditions (1% v/v H_2 in air) and in powder form in kinetic conditions for comparative purposes.

1. Introduction

Hydrogen has been proposed as one of the most desirable and efficient energy carriers for the implementation of a more sustainable energetic paradigm. It has an attractive energy density (142 MJ kg^{-1} while for liquid hydrocarbons it is 47 MJ kg^{-1}) and once obtained through green resources, can produce energy upon generating water as the only by-product.[1–3] Catalytic hydrogen combustion (CHC, reaction (1)) is a key reaction in the "hydrogen economy" because it is safe, controllable and highly exothermic (−286 kJ mol^{-1}).[3]

$$H_2 + \tfrac{1}{2}O_2 \rightarrow H_2O \qquad (1)$$

This reaction can be employed for heat production (heaters, cookers) as well as safety purposes (elimination of undesired hydrogen).[4–10] Regarding safety, the scale of H_2 managed can range from the elimination of the large amounts generated in the nuclear industry (in case of an accident), to the byproducts of chemical and petrochemical industries, or to the exhaust gases from fuel cells.[6–10] According to literature, the utilization of hydrogen is always less than 95% even in the latest fuel cells developed for vehicles, and the residual hydrogen is discharged in the exhaust gases.[7] The accumulation of hydrogen may result in the formation of explosive combustible mixtures. For this reason the study of CHC is an important field of application.

Catalytic hydrogen combustion is safer and more controllable than flame combustion, since the reaction only occurs on the catalyst's surface. Pt and Pd are the most active catalysts for (1) and permit to initiate the reaction without ignition even at room temperature.[11] For the design of heating or safety devices based on CHC, the preparation of supported catalysts is essential, since it prevents aggregation and permits to reuse them more easily. Silicon carbide (SiC) has recently been proposed as an advantageous support for exothermic reactions for many reasons, especially because it has high thermal and chemical resistance, mechanical strength and high thermal conductivity (which prevents the formation of hot spots).[12] Synthesis of SiC has developed very fast since the late 90s when several research groups focused on obtaining and using porous β-SiC with surface areas ranging from 30 to 80 m^2 g^{-1}, significantly higher than that of the α-SiC phase (~1 m^2 g^{-1}).[12,13]

Biomorphic SiC (bio-SiC) are porous SiC scaffolds obtained by reactive infiltration with liquid Si of wood-derived carbon.

[a]Instituto de Ciencia de Materiales de Sevilla (CSIC-Univ. Sevilla), Avda. Américo Vespucio 49, 41092-Sevilla, Spain. E-mail: asuncion@icmse.csic.es; gisela@icmse.csic.es

[b]Departamento Física de la Materia Condensada, Universidad de Sevilla, Avda. Reina Mercedes S/N, 41012 Sevilla, Spain

Due the nature of the synthesis method, the resulting SiC material mimics the microstructure of the original wood precursor, allowing a large number of porous microstructures to be obtained by simply choosing wood of adequate species.[14–17] This is also a near net-shape process, meaning that components with complex geometries can be obtained by machining the carbon preformed pieces prior to infiltration, instead of the final SiC monolith, significantly lowering processing costs.

The anisotropic, interconnected nature of the porosity in biomorphic SiC has been extensively studied for a range of applications that involve or require fluid flow, either liquid or gas, such as gas filtration in high temperature gasification of biomass[18–20] or as a catalyst support,[21–23] where it has shown a significant improvement over conventional SiC supports.

In a previous paper[24] we investigated the use of a SiC foam as support for a Pt washcoat (both support and catalyst from commercial suppliers). The CHC reaction was studied to determine the kinetic parameters for the proposed SiC/Pt monolithic material. In the present paper we have studied the CHC in conditions of excess of oxygen, simulating the H_2 concentration of the exhaust gas from a fuel cell (3–4% v/v H_2/air mixture). We have prepared and used bio-SiC based monoliths as catalyst supports for the first time for this reaction. Capillary forces on the monoliths were exploited for the incipient impregnation of chloroplatinic acid solutions (H_2PtCl_6, CPA). Different conditions of impregnation (solvent, Pt loading) were explored together with drying methods (oven, freeze drying) and their influence on the active phase distribution was evaluated. The catalytic activity of the prepared catalysts was evaluated at different H_2/air mixture flowrates and H_2 concentrations. In addition to our previous studies,[24] referred to porous SiC with isotropic pore distributions, an objective in this work was to explore the anisotropic nature of porosity in bio-SiC. Therefore temperature at different points of the monoliths and thermal conductivity measurements are presented and discussed under diffusional regime conditions (100% conversion for the CHC reaction). Catalytic activity was also measured in less than 100% conversion conditions for comparative purposes.

2. Experimental

2.1. Supports' preparation

Porous, biomorphic SiC supports were prepared using a method previously described elsewhere[25–27] and schematized in Fig. 1. In brief, wood samples of the chosen precursors were pyrolyzed in flowing N_2 at a temperature of 1000 °C in a tube furnace, yielding porous carbon monoliths. Obtaining crack free monoliths required the use of slow heating rates: 1 °C min^{-1} from room temperature to 500 °C, and 5 °C min^{-1} from 500 °C to 1000 °C, holding time was 30 minutes in all cases. The resulting carbon monoliths were then machined into disks 30 mm in diameter and 5 mm thick and further infiltrated with liquid silicon in a vacuum furnace at 1450 °C. As a result, biomorphic SiC/Si disks were obtained containing a continuous β-SiC phase mimicking the original wood microstructure, with residual Si filling the pores. This silicon was subsequently removed by wet etching using a solution of HNO_3 and HF in a molar ratio of 2/3 in distilled water under magnetic stirring for 48 h. The resulting porous SiC monoliths were finally washed several times until neutral pH and then dried.

Three different wood precursors were deemed representative of the variety of available microstructures and chosen for this study: pine fir wood (*Abies Alba*) was chosen as a representative of softwoods and resulted in a porous SiC support containing a monomodal, well dispersed channel distribution;[15] sapele wood (*Entandrophragma cylindricum*) as a representative of hardwoods yielding a porous SiC support with a bimodal channel distribution of large sap channels and smaller cell vessels;[28] and Medium Density Fiberboard (MDF) as a representative of recycled wood products, which consists of hot-pressed wood fibers.[29] A commercial alumina bonded SiC foam (from Lanik s.r.o.), which contains 80 pores per inch, was employed for comparison. Further characterization of this foam can be found in ref. 24.
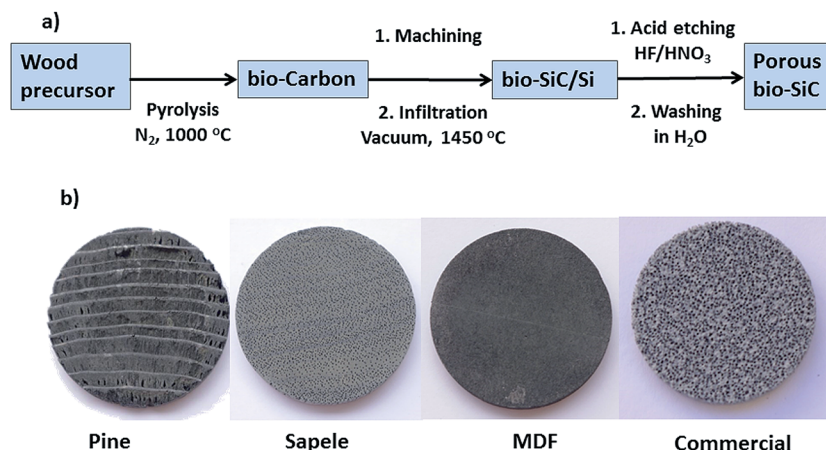

Fig. 1   (a) Scheme of the fabrication process of bio-SiC monoliths. (b) Photographs of the prepared bio-SiC based monoliths compared to the commercial SiC.

2.2. Catalysts' preparation

Bio-SiC (from sapele, pine or MDF) supported catalysts were prepared by pore volume impregnation of the support with aqueous or ethanolic H_2PtCl_6 (CPA, Sigma Aldrich) solutions. The Pt loading was calculated for a final amount of 0.25, 0.5 or 1.5 wt% as will be indicated in the text. The pore volume was first measured for each type of support (sapele, pine or MDF) in duplicate. Chloroplatinic acid was dissolved in the desired volume of the indicated solvent and placed in a 31 mm diameter flask. Monoliths were placed in the flask and solvent was absorbed by capillary forces. After some minutes, surface of monoliths appeared wet. The monoliths were left during 30 min in contact with the impregnating solution and then were extracted. The slight excess of solution was removed by placing the monolith in absorbent paper and then they were left to dry at room temperature during 4 h (except those further freeze dried). The drying procedure was varied in order to study its effect on Pt final distribution. Those monoliths impregnated using water as solvent were either conventionally treated in an oven (denoted as aqueous in the text) or freeze dried to eliminate the solvent. Monoliths impregnated with ethanol (denoted as ethanolic) were also dried in the oven. Those monoliths dried in the oven were treated at 120 °C overnight in static air. Freeze-drying was performed immediately after impregnation and treatment lasted 12 h. All monoliths were then calcined in static air at 400 °C during 4 h (with 3 °C min⁻¹ heating ramp).

For comparison, a commercial SiC foam (from Lanik s.r.o.)[24] supported catalyst (0.5Pt/commercial) was prepared by impregnation with an ethanolic solution of H_2PtCl_6 for a final Pt loading of 0.5 wt%. This catalyst was dried in the oven and further calcined in the above mentioned conditions.

2.3. Characterization of bare and catalysts loaded supports

The density of bio-SiC supports was obtained by means of helium pycnometry (Micromeritics Accupyc) complemented with geometrical measurements. BET surface area of prepared supports was measured but results showed values below 1 m² g⁻¹ in all cases. These results were confirmed by Hg porosimetry which showed pore sizes in the μm to tens of μm range.

Thermal diffusivity was measured on bare SiC supports at room temperature using the laser flash heating technique (LFA1600, Linseis) in vacuum. Samples were disks of the same thickness as the catalytic supports but with a slightly smaller diameter to fit into the largest sample holder available. To determine the thermal anisotropy, samples were prepared in two different orientations: one which was called 'axial', where the disk axis was parallel to the gas flow direction in the catalytic experiments (which coincided with the elongation of the wood channels and the pressing direction in MDF) and another one described here as 'radial' where the disks' axes were perpendicular to the gas flow direction. In this way, we could measure the thermal conductivity anisotropy of the different supports. To avoid any direct laser beam going through the porous supports and distorting our measurements, samples were coated with graphite spray. Thermal conductivities were then calculated from the diffusivities using the relation $K =$

$\rho C_v \alpha$ where ρ and α are the sample's measured density and diffusivity, respectively, and C_v is the SiC heat capacity which was taken from ref. 30.

SEM analyses were performed on the monolithic catalysts in a high resolution SEM-FEG microscope Hitachi S4800 operating at 5 keV or in a conventional JEOL 6460-LV SEM at 20 keV. The Hitachi S4800 microscope is equipped with a Bruker X-Flash 4010 EDX detector and a backscattering electron (BSE) detector for specific analysis in this work.

For TEM studies, pine based bio-SiC samples were first ground into a powder, dispersed in ethanol by ultrasound and dropped on a copper grid. TEM measurements were performed at 300 kV on a FEI FEGTEM Tecnai G2 F30 microscope.

X-ray diffraction measurements were performed using the Cu Kα radiation in a Siemens D5000 diffractometer in a Bragg–Brentano configuration in the 2θ angle range of 40–80 degrees. The quantitative crystallite size analysis was done with the software X'Pert Highscore Plus from PANalytica B.V.

Pulse chemisorption measurements were performed on an AutoChem 2920 chemisorption analyser from Micromeritics.

For plasma ICP measurements samples were sent to two independent laboratories but complete SiC digestion was not achieved and thus the obtained loadings are not reliable. The Pt loading was estimated from exact amounts of Pt precursor in the pore volume impregnation methodology used in this work.

2.4. Catalytic tests

Catalytic tests were performed in a homemade reactor specially designed to test monolithic pieces of 30 mm diameter and 5 mm thickness. Above the monolith there is some space for the gas inlet (H_2 and air in separate opposite entrances) which is filled with glass wool in order to facilitate gas mixing. Reactions were carried out with a feed mixture consisting of 200, 400 and 1000 ml min⁻¹, of a 3% v/v H_2/air mixture during one hour each. During the fourth hour the reactor was fed with 1000 ml min⁻¹ of a 4% v/v H_2/air mixture. These conditions are far from the kinetic regime. The H_2 concentration was selected to simulate the hydrogen concentration in the exhaust gas from a fuel cell, and the heat released is high enough to produce increase in monoliths' temperature, achieving the diffusional regime for all the total mixture flows used. These conditions would permit to detect the formation of hot spots and to correlate temperature distribution with thermal anisotropy measurements. Catalysts were tested with no previous conditioning treatment. Temperature was measured by a series of K-type thermocouples placed at different parts of the monolith as it will be indicated later.

To get further information from the Pt-impregnated monoliths, catalytic tests were done in conditions of low H_2 conversion (<100%). In this case, the reactor was fed with 200 and 600 ml min⁻¹, of a 1% v/v H_2/air mixture during 4 h and 1 h respectively. Before testing, all samples were reactivated to get 100% conversion with a gas fed of 1000 ml min⁻¹ of a 4% v/v H_2/air mixture and left cooling to room temperature.

Additionally, some experiments were done in kinetic regime with samples first ground into a powder as described in the

caption of Fig. S2 (ESI†). Dilution with bare support is needed to study the kinetic regime range.

The exhaust gas was analyzed using a HP 5890 chromatograph. Hydrogen conversion was followed by measuring H_2 amount as a function of time by using a ShinCarbon® packed column and a thermal conductivity detector. N_2 was used as the carrier gas.

3. Results and discussions

3.1. Supports' and catalysts' characterization

3.1.1. The supports. The microstructure of the obtained porous bio-SiC monoliths is shown in Fig. 2, at low and high magnifications. Due to the presence of growth rings in natural wood, inhomogeneities can be detected especially in the case of pine-derived SiC, where growth rings can also be clearly appreciated in Fig. 1b. The microstructure of the commercial SiC foam is also shown in Fig. 2 for comparison purposes. This material is cellular and essentially isotropic, consisting of roughly overlapping spherical pores (characteristic pore diameters 300–500 μm). In the case of the wood derived bio-SiC monoliths different microstructures are observed. In the case of pine, pores are cylindrical and form channels that go through the disk and have a quite monodisperse diameter distribution (characteristic diameters 15–60 μm), with some denser bands that correspond to the above mentioned growth rings which can be also seen in the top-left panel of Fig. 2. Sapele-derived bio-SiC, on the other side, shows a bimodal distribution
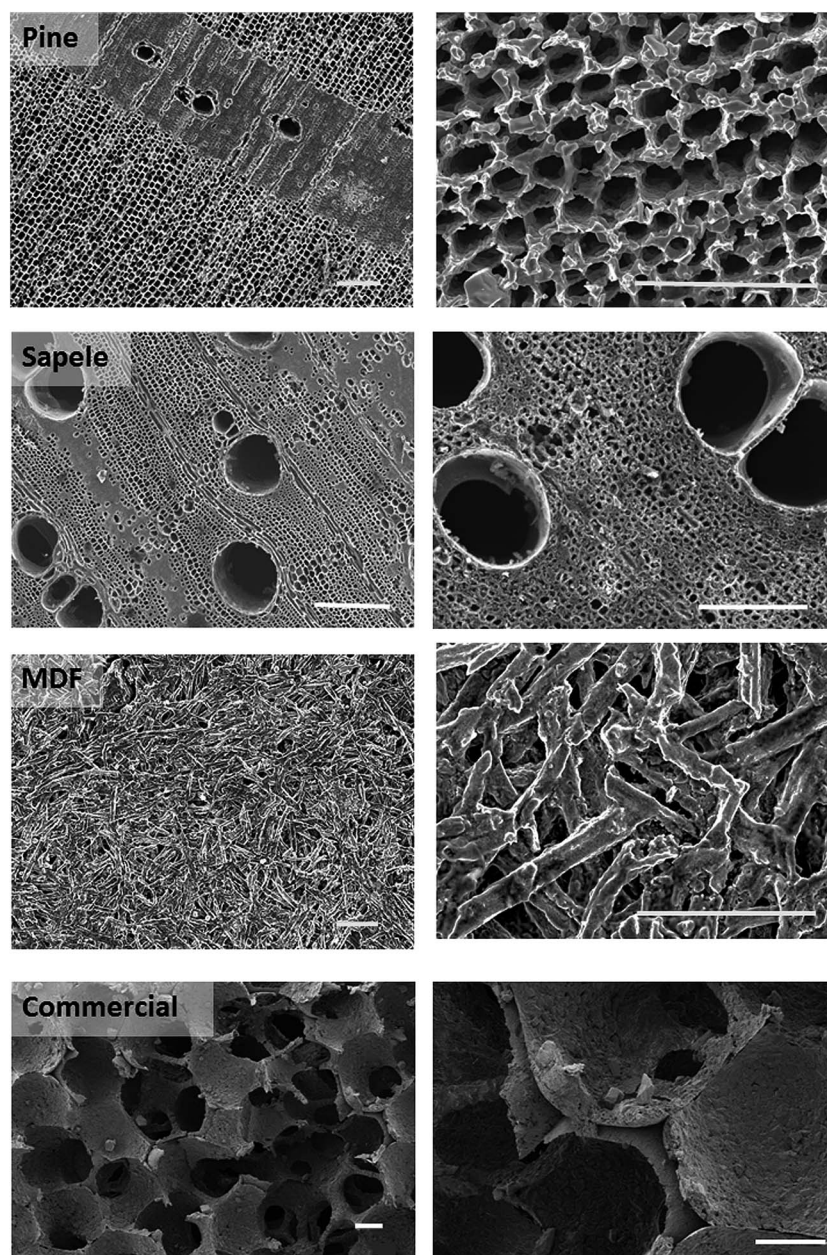

Fig. 2 SEM images of the prepared bio-SiC monoliths based on wood in comparison to the commercial SiC (foam). Scale bar: 200 μm.

characteristic of gymnosperm wood, with wider sap channels (characteristic diameters 20–200 μm) embedded in a matrix of narrower pores (characteristic diameters 1–15 μm). The case of MDF-derived SiC is different from the previous two, since MDF is a recycled wood product obtained by pressing of wood fibres. Its microstructure thus consists of SiC fibres which are packed so that their longest direction is perpendicular to the pressing direction, to which we refer as "axial" in this paper.

Table 1 shows the porosities, densities and thermal diffusivities and conductivities for all the samples studied. In the case of the Lanik commercial SiC foam, conductivity is essentially isotropic, whereas for the wood derived SiC samples there is a marked anisotropy in thermal conductivities. Pine derived SiC shows the highest anisotropy, conductivity being larger in the axial direction by a factor of over two, whereas sapele derived SiC is closer to isotropic but still has a higher conductivity in the axial direction. Due to its microstructure the case of MDF derived SiC is different: in this case the anisotropy ratio is smaller than one, meaning that conductivity is larger in the radial than in the axial direction. This behaviour was expected given the transversely isotropic packing of the wood fibres during MDF processing as well as their aspect ratio, features that translate to the bio-SiC support.

Sapele and MDF derived SiC monoliths are denser and more difficult to break than the pine derived ones. This is due to the high porosity and the inhomogeneous distribution of the axial channels between the growth rings of the latter. For fundamental studies, pine derived SiC monoliths can be very easily converted into powder. They were chosen for the studies of active phase distribution which are discussed in the following section. For practical applications, MDF and sapele derived monoliths are more advantageous in respect to their mechanical strength.

3.1.2. The catalysts. Study of Pt distribution as a function of the preparation method. For exothermic reactions, it is essential to achieve homogeneous active phase distribution on the complete scale of the monolithic structure. This requirement, together with the high thermal conductivity of the SiC based support, contributes to prevent the formation of hot spots. The formation of hot spots can affect the selectivity (as occurs for the Fischer–Tropsch reaction) or the safety of any

reaction based in combustion (explosion temperatures should never be reached). It is known that when impregnating an active phase in porous solids, heat treatment tends to redistribute the macroscopic active phase due to capillary suction, resulting in the accumulation of the former in the outer shell of the monolithic structure.[31] For this reason, those monoliths impregnated with water and ethanolic Pt solutions (0.5 or 0.25 wt% Pt final loading) were dried in static air (samples labelled 0.5 or 0.25Pt/pine-aqueous and 0.5Pt/pine-ethanolic) and compared with the freeze dried sample after impregnation with an aqueous CPA solution (labelled 0.5Pt/pine-freeze drying). SEM/EDX measurements were performed to evaluate, in a macroscopic scale, the accumulation of platinum as schematized in Fig. 3. Monoliths were divided into 9 positions and SEM analyses of (2.5×2) mm^2 areas were carried out with an incident electron beam from the top. The amounts of Si and Pt
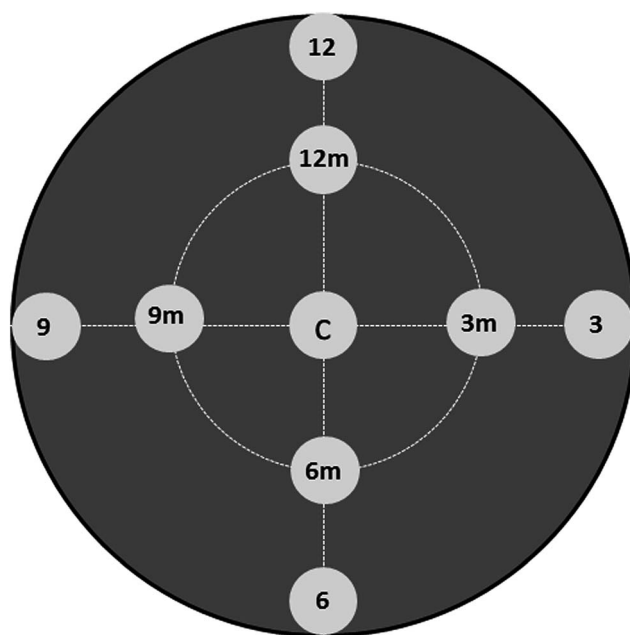

Fig. 3 Scheme of SEM/EDX measurements performed on Pt catalysts over monolithic bio-SiC supports in order to evaluate the macroscopic active phase distribution.

Table 1 Porosity, bulk density and room temperature thermal conductivity parameters for the SiC supports studied in this work

	Pine	Sapele	MDF	Commercial[a]
Porosity (%)	56	52	46	83
Bulk density (g cm^{-3})	1.40	1.54	1.73	0.55
Axial thermal diffusivity (cm^2 s^{-1})[b]	0.60	0.42	0.31	0.03
Radial thermal diffusivity (cm^2 s^{-1})[b]	0.25	0.33	0.40	
Axial thermal conductivity (W mK^{-1})[b]	54	38.5	34	1.23
Radial thermal conductivity (W mK^{-1})[b]	22	29.8	43	
Thermal conductivity anisotropy ratio[b]	2.4	1.3	0.8	1

[a] Details of this support can be found in (ref. 24). [b] Axial diffusivities and conductivities were measured along the supports' axes, which coincided with the direction of gas flow in the hydrogen combustion experiments. The thermal conductivity ratio is simply the ratio of axial to radial conductivity: a value of unity corresponds to a nominally isotropic sample, whereas a value higher than one means that the conductivity is higher in the axial than in the radial directions.
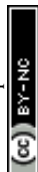
Table 2 Pt and Si percentages (mass%) obtained by SEM–EDX analysis for the indicated samples according to positions depicted in Fig. 3

Position	0.5% Pt/pine-aqueous		0.5Pt/pine-freeze drying		0.5Pt/pine-freeze drying 180°		0.5Pt/pine-ethanolic	
	% Si	% Pt	% Si	% Pt	% Si	% Pt	% Si	% Pt
12	95.2	4.8	94.5	5.9	94	6	93.2	6.8
12m	96.3	3.7	95.9	4.1	—	—	70	30
3	97.4	2.6	94.1	5.5	94.8	5.2	87	13
3m	96.7	3.3	94.7	5.3	—	—	80	20
6	95.6	4.4	97.6	2.4	96.4	3.6	90.4	9.6
6m	97.2	2.8	97.6	2.4	—	—	77.3	22.7
9	43.9	56.1	95.8	4.2	96.2	3.8	88.9	11.1
9m	83.9	16.1	96.5	3.5	—	—	89	11
Centre	95.8	4.2	96.9	3.1	97.6	2.4	93.7	6.3
Average	—	11 ± 6	—	4.0 ± 1.3	—	4.3 ± 1.7	—	15 ± 8
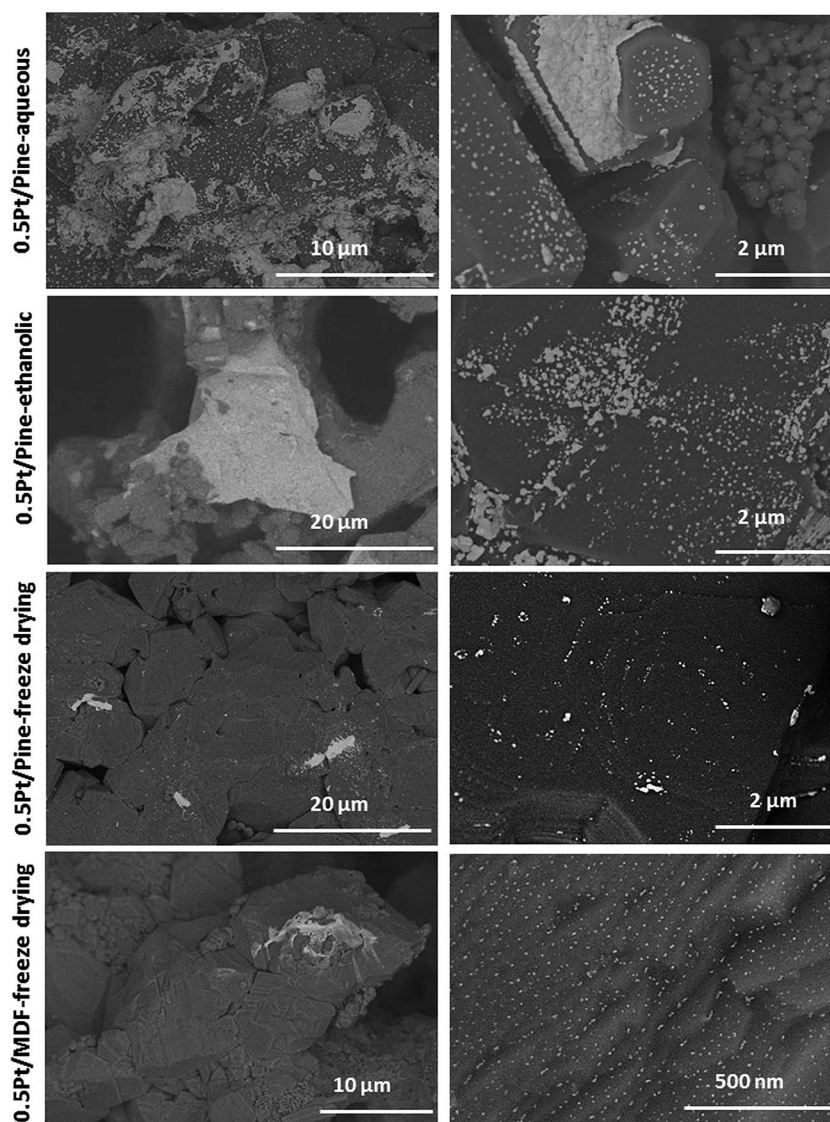
Fig. 4 Representative SEM micrographs (BSE images) of the Pt impregnated catalysts on bio-SiC using different impregnating solvents and drying methods (as indicated in left hand side of the figure). High magnification images at the right hand side.

were quantified by EDX in each position (quantification of carbon by EDX is not accurate because it is a light element). Table 2 shows the results for different monoliths prepared at the indicated conditions. The study of the variation of Pt amount (mass% referred to a total 100% for Si + Pt) as a function of the position and the standard deviation on the average composition shows that samples dried in an oven, with 0.5 wt% Pt (either impregnated with water or with ethanol), exhibit large compositional variations and a high accumulation of Pt at the outer shell of the monolith. In the case of the freeze dried sample (0.5Pt/pine-freeze dried) the composition is more homogeneous. This latter sample was also studied by EDX from the back side, a rotation of 180° was performed and Pt amount was quantified in the same positions. Local and average Pt mass% compositions indicate a homogenous distribution on both sides of the monolith for the freeze dried sample.

Fig. 4 shows representative SEM images, taken from the top in the centre of each monolith (as shown in Fig. 3), for the Pt impregnated catalysts on pine derived SiC by the different preparation methods. It is clear that conventional drying methods in an oven (for both water or ethanol impregnated catalysts) produce higher number and size of Pt aggregates accumulated at the monolith outer shell (white patches in the images). In this sense, the freeze dried samples contains smaller and more isolated aggregates (Fig. 4). Nevertheless in all samples, Pt aggregates were found especially on the growth rings. The MDF derived bio-SiC was also Pt impregnated and freeze dried for comparison, and SEM images are also shown in Fig. 4. The distribution of the active phase is very similar to the one for the 0.5Pt/pine-freeze drying sample. Higher magnification SEM images (right hand side of Fig. 4) show that all prepared materials exhibit zones in which small and disperse particles (white dots) can be found. These small particles are located in the flat surfaces of the SiC crystals without defects. Edges, terraces, grain boundaries and stacking faults seem to accumulate more Pt aggregates.

Fig. 5 shows additional micrographs of the 0.5Pt/pine-freeze dried sample studied by SEM. Fig. 5a shows a planar view image on top of a channel wall. Even in this zone, where a large accumulation of defects in the substrate is observed, small and disperse Pt aggregates (white spots) are found. The study of the Pt distribution in cross-sectional views (channel axial direction) is shown in Fig. 5b. A high degree of dispersion is also found demonstrating the effectiveness of the freeze drying method to obtain a more homogeneous distribution of the metallic phase, and therefore reducing its accumulation at the outside surface of monoliths. Our results are in agreement with previous works[31,32] also showing that the most homogeneous macroscopic active phase distribution was obtained by freeze drying, microwave drying and the deposition-precipitation method. Static and forced air drying produced however, stronger precursor accumulations.

3.1.3. Microstructure and Pt crystallite size. Fig. 6 shows XRD measurements of the catalysts prepared on pine derived bio-SiC supports, ground into powder. First of all, it is clear from the diffractograms the presence of the diffraction peaks at 35.6, 41.3, 60.0, 71.7, and 75.4 degrees (2θ) corresponding to the crystal planes of β-SiC (ICDD 00-029-1129) (Fig. 6a). The broad
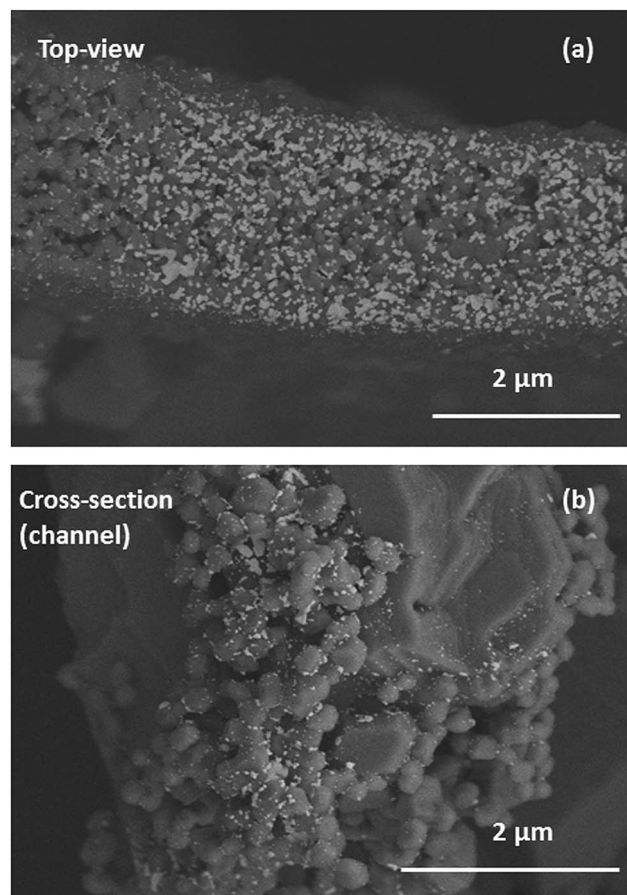

Fig. 5 Representative SEM micrographs (BSE images) of the 0.5Pt/pine-freeze drying sample in top view (a) and cross section (b) (inside a channel).

peaks attributed to metallic Pt phase are also shown in Fig. 6a. The signal (indicated by an arrow) corresponding to the (111) plane at $2\theta = 39.6°$ of metallic Pt was used to calculate average crystallite size by the Scherrer's equation and results are shown in Fig. 6b. Pt crystallites (including particles and aggregates) are medium to big size in all cases (33–49 nm). This result is not surprising because the hydrophobic character of SiC does not favour metal–support interactions.[33] In the case of the 0.25 wt% Pt conventionally impregnated sample, average size was not calculated due to the small signal.

Particles were also observed by TEM for the monoliths ground into powder. The powder was obtained from the space between growth rings. Fig. 7 shows some representative micrographs of the 0.5 wt% Pt catalysts prepared on pine derived bio-SiC. The SiC crystal grains are clearly observed, as well as characteristic Pt particles and some aggregates of different sizes, as expected from the SEM data and in agreement with the average crystallite sizes determined by XRD analysis.

Nitrogen sorption measurements in this type of SiC macroporous monoliths have shown very small surface areas. Hydrogen chemisorption was therefore performed to characterize the Pt active phase supported on pine derived bio-SiC materials also in comparison to the commercial support.
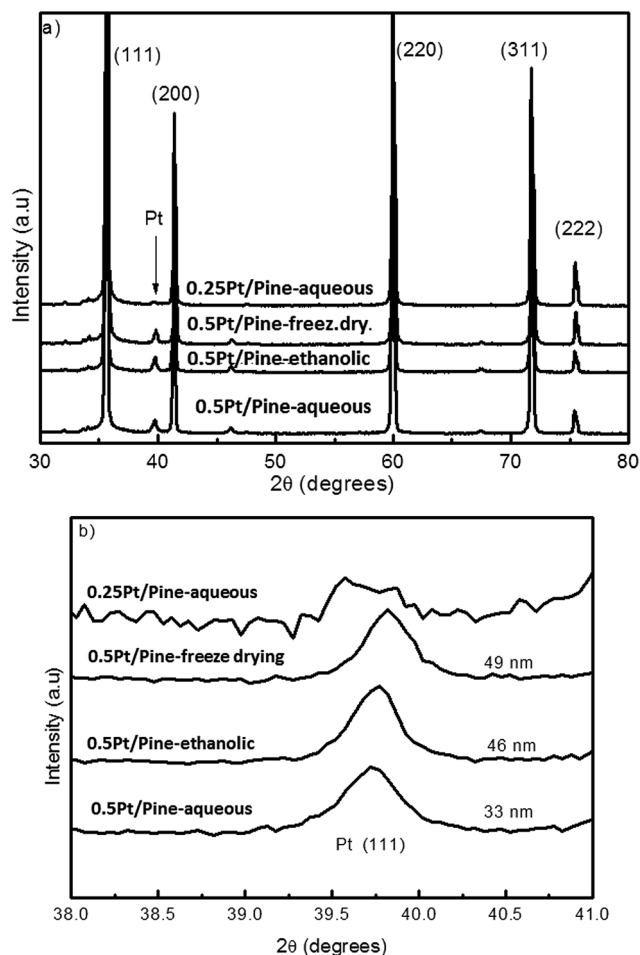
Fig. 6 (a) XRD measurements for the Pt catalysts deposited on pine based bio-SiC under different conditions as indicated in the figure; (b) region of the (111) plane of Pt.

Metal surface areas were found in the range of 7 to 14 m^2 g_{metal}^{-1} as expected from Pt particles of medium to big size as already shown by SEM, XRD and TEM measurements. These data are presented in Table 4 and discussed in sub-section 3.2.2.

3.2. Catalytic activity

3.2.1. Experiments in diffusional regime. Temperature distribution profiles and catalyst's durability. Total conversion for reaction (1) was measured in conditions of excess of oxygen

for all samples over two start–stop cycles. First the reactor was fed with a 3% v/v H_2/air mixture at 200, 400 and 1000 ml min^{-1} during 1 hour respectively. Then the H_2 concentration was increased to 4% v/v for a total mixture flow of 1000 ml min^{-1} and the reaction was carried out for a fourth hour and then stopped. Second cycle was carried out under identical conditions. During the reaction, the temperature was monitored by thermocouples inserted in different points of the monolith as shown in Fig. 8a. In all the experiments, a steady state in conversion was achieved after 5 minutes of reaction. Conversions are shown in Table 3. In all cases, conversion was very high and close to 100% even for the 200 ml min^{-1} H_2/air mixture flowrate. Despite the reactor is fed with room temperature gas mixtures, conversion increases with mixture flowrate for all monoliths. In these conditions (high H_2 concentration), the heat released is high enough to produce an increase in temperature and thus maintain the high conversion. This behaviour is usual in very exothermic reactions. Catalyst loading could be reduced to 0.25 wt% Pt with no detriment in conversion. The 0.25Pt/pine-aqueous catalyst fed with 1000 ml min^{-1} of 4% v/v H_2 mixture was able to convert as much as 4.8 liter H_2 min^{-1} g_{Pt}^{-1}. The performance of all catalysts was maintained in the second cycle.

The comparison of the prepared catalysts with literature is not an easy task, since it is difficult to find reports in which monolithic catalysts (type and shape of monolith, active phase, metal loading, etc.) and testing conditions (reactor geometry, H_2 concentration, equivalence ratio, etc.) are exactly the same as the ones presented here. A Pt-based catalyst (1 wt% Pt) was reported before on a $Ce_{0.6}Zr_{0.4}O_2$/$MgAl_2O_4$ mesoporous monolithic support and tested under H_2/air (4% H_2) mixture with similar conversion as herein.[7] Also a Pt catalyst on porous ceramic support has achieved similar conversion as herein in a micro combustor (10 × 10 × 1.5 mm) with Pt loadings in the range of 0.4–3.7 wt% Pt, but with different H_2/O_2 equivalence ratio (=1).[6]

Achieving almost 100% conversion in all samples is ideal to study temperature distribution because the amount of heat released is similar and permits to correlate temperature with thermal conductivities. Temperature was monitored in different points of the monoliths as represented in Fig. 8a: T2 at the top-center, T1 at the top-side, and T3 at the lateral-edge. Results are shown in Fig. 8 for freeze dried samples which
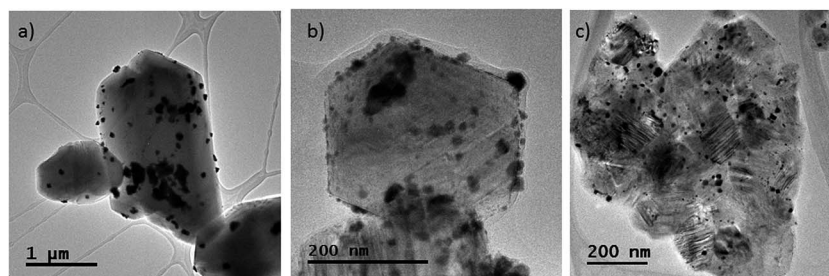

Fig. 7 Representative tem images of the 0.5 wt% Pt catalysts prepared on pine derived bio-SiC: (a) aqueous conventional drying; (b) ethanolic conventional drying; (c) aqueous freeze drying.
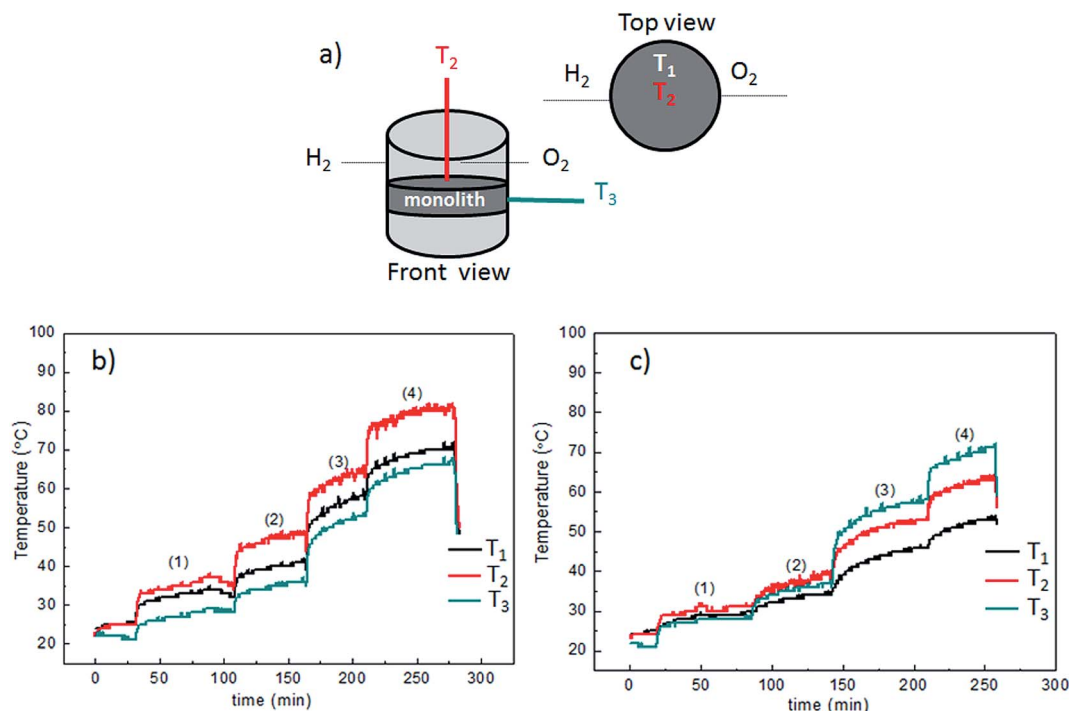
Fig. 8 Catalytic measurements on the Pt impregnated monoliths. (a) Scheme of the reactor and position of thermocouples. Temperature profiles for the: (b) 0.5Pt/pine-freeze drying sample; (c) 0.5Pt/MDF-freeze drying sample. (1): Mixture 200 ml min^{-1}, 3% H$_2$ v/v; (2): mixture 400 ml min^{-1}, 3% H$_2$ v/v; (3): mixture 1000 ml min^{-1}, 3% H$_2$ v/v; (4): mixture 1000 ml min^{-1}, 4% H$_2$ v/v.

Table 3 Steady state conversion for the studied catalysts as a function of the H$_2$/air mixture flowrate, H$_2$ concentration and cycle number

	% conversion							
	Cycle 1				Cycle 2			
	200 ml min^{-1}	400 ml min^{-1}	1000 ml min^{-1}	1000 ml min^{-1}	200 ml min^{-1}	400 ml min^{-1}	1000 ml min^{-1}	1000 ml min^{-1}
Sample	3% H$_2$ v/v	3% H$_2$ v/v	3% H$_2$ v/v	4% H$_2$ v/v	3% H$_2$ v/v	3% H$_2$ v/v	3% H$_2$ v/v	4% H$_2$ v/v
0.25Pt/pine-aqueous	100	100	100	100	100	100	100	100
0.5Pt/pine-aqueous	100	100	100	100	100	100	96	96
0.5Pt/pine-freeze drying	97	100	100	100	97	100	100	100
0.5Pt/pine-ethanolic	100	100	100	100	95	100	100	100
0.5Pt/sapele-freeze drying	96	95	100	100	96	96	100	100
1.5Pt/sapele-aqueous	99	99	99	100	99	100	100	100
0.5Pt/MDF-freeze drying	95	100	100	100	100	100	100	100

	Cycle 3			Cycle 4		Cycle 5
	200 ml min^{-1}	1000 ml min^{-1}	1000 ml min^{-1}	200 ml min^{-1}	1000 ml min^{-1}	1000 ml min^{-1}
Sample (stored in air for 8 months)	3% H$_2$ v/v	3% H$_2$ v/v	4% H$_2$ v/v	3% H$_2$ v/v	4% H$_2$ v/v	4% H$_2$ v/v
0.5Pt/pine-freeze drying	51	91	94	85	96	100

have been selected from their more homogeneous Pt distribution, a requirement to avoid the formation of hot spots.

Temperature profiles, as a function of time, were plotted in Fig. 8b for the 0.5Pt/pine-freeze dried sample. During the whole experiment, the temperature trend was T2 > T1 > T3, which is a reasonable temperature distribution for a homogeneously distributed active phase on an anisotropic monolith such as the pine-derived bio-SiC (conductivity being larger in the axial direction). Fig. 8c shows the temperature profiles for the 0.5Pt/MDF-freeze dried sample. At a low amount of H_2 converted (200 ml min^{-1} mixture flow) the relative temperatures show small differences with the trend T2 > T1 > T3. However, as the total volume of H_2 converted is increased, the value of T3 starts to increase respect to the rest of temperatures to reach a clear trend T3 > T2 > T1 at 1000 ml min^{-1} of 4% v/v H_2/air mixture. This result can be attributed to the larger conductivity in the radial rather than in the axial direction in the case of the MDF support.

The durability of the 0.5Pt/pine-freeze drying catalyst was tested after 8 months of storage in air. In a third cycle (8 months after the first and second cycles), the catalyst was fed with 200 ml min^{-1} of a 3% v/v H_2/air mixture during 1 hour, then with 1000 ml min^{-1} of a 3% v/v H_2/air mixture during another hour, and finally with 1000 ml min^{-1} of a 4% v/v H_2/air mixture during a third hour (Table 3). The achieved steady state conversions were 51, 91 and 94%, respectively. However, in a fourth cycle (near in time with the third), the conversion at low mixture flow (200 ml min^{-1}) reached 85% and at high mixture flow was 96% (4% v/v 1000 ml min^{-1}). Two conclusions can be extracted from these data. Firstly, at a low mixture flow (200 ml min^{-1}) catalyst deactivates around 50% upon 8 months air storage. However, at a high mixture flow this effect is not so pronounced. Secondly, high conversion and temperature operation can be achieved feeding the reactor with 4% H_2/air mixture at 1000 ml min^{-1} which permits to recover the activity almost similar to the initial one in subsequent cycles. This means that operation at high conversion conditions permits to reactivate the catalyst stored under air conditions for long periods.

The 0.5Pt/pine-freeze drying sample was also tested in a long life experiment. In a fifth cycle (near in time with the third and

the fourth), the monolith was fed with 1000 ml min^{-1} of a 4% v/v H_2/air mixture during $ca.$ 7 hours of continuous use. In the previous 20 min of the experiment ($t < 0$) the reactor was fed with 200 ml min^{-1} of a 3% v/v H_2/air mixture just to start heating the system. The plot of the conversion as a function of time is found in Fig. 9a. From the plot it is clear that stable 100% conversion is reached and maintained during the whole experiment. The temperature profile in Fig. 9b shows that steady state is achieved after $ca.$ 1 hour operation. The temperature trend is T2 > T1 > T3 which confirms the anisotropy in thermal conductivity of the pine derived bio-SiC as discussed above.

3.2.2. Experiments in low conversion conditions. Kinetic regime.
Activity of the prepared monoliths was tested in low H_2 conversion conditions (200 and 600 ml min^{-1} of 1% v/v H_2/air mixture). Results are shown in Table 4. Steady state conversion was not achieved as fast as in diffusional conditions (an example shown in Fig. S1 in ESI†). Except for the 0.5Pt/pine-aqueous sample, which was the most active, less than 100% H_2 conversion was measured in all cases. Table 4 also summarizes crystallite size (from XRD) and shows the active particle diameter (from H_2 chemisorption) for the compared catalysts. The 0.5Pt/commercial sample was also included for comparison with a isotropic commercial support. What is clear from these results is that freeze-drying is the most efficient method to disperse active phase at macroscopic and microscopic levels, showing the highest metallic surface area (14 m^2 g^{-1}, Table 4). However, structure–activity comparisons cannot be made in our conditions because samples are very heterogeneous in Pt particle size. This fact is evidenced by differences in crystallite size (Scherrer) and active particle diameter (H_2 chemisorption). Both techniques show average results but the former overestimates the contribution of higher crystallite sizes while the latter the smaller particles.

Unlike in diffusional regime, the increase in the total H_2/air mixture flowrate on the monolithic catalysts does not produce an increase in H_2 conversion. This effect is indicative of kinetic control. These low conversion (and thus low heat release) conditions are not adequate for the study of thermal properties of our monoliths, since the heat released by the reaction is not constant amongst samples and the cooling effect of the feeding
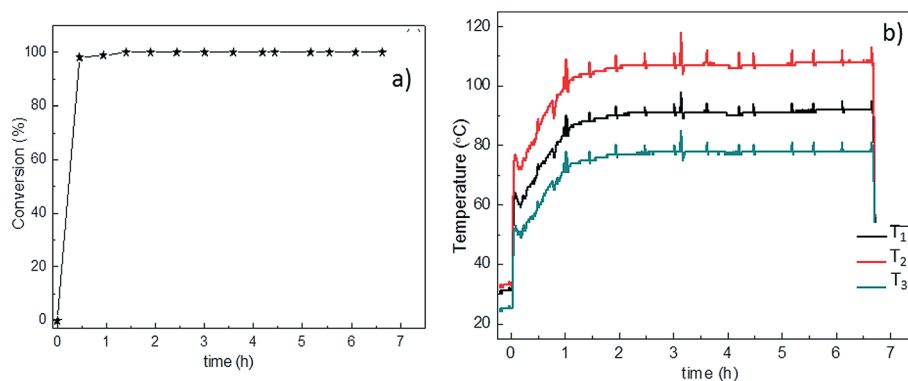

Fig. 9 Stability of the 0.5Pt/pine-freeze drying catalyst in a long life (7 h) experiment. (a) Conversion as a function of time (b) temperature profile at the positions defined in Fig. 8a.
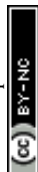
Table 4 Steady state conversion for the catalysts under 1% v/v H_2/air mixture. Characterization of the Pt active phase by H_2 chemisorption and X-ray diffraction

Sample	% conversion		H_2 chemisorption analysis		XRD
	200^a ml min^{-1}	600^a ml min^{-1}	Metallic surface area (m^2 g^{-1})	Active particle diameter (nm)	Crystallite size (Scherrer) (nm)
0.5Pt/pine-freeze drying	69	53	14	20	49
0.5Pt/pine-aqueous	100	85	6	45	33
0.25Pt/pine-aqueous	87	70	7	41	—
0.5Pt/commercial	79	79	7	41	57

^{a} 1% v/v H_2/air gas mixture.

mixture (supplied at room temperature) gains special relevance. This can be evidenced by the temperature profiles for the 0.5Pt/pine freeze drying sample in Fig. S1 (ESI†).

To give a better idea of the efficiency of the herein presented catalysts, activity was tested for materials in powder form in a tubular reactor (1% v/v H_2/air, 200 ml min^{-1}). Conversion vs. temperature curves were measured in cooling mode and results are shown in ESI Fig. S2† (T_{50} is defined as the temperature for 50% conversion). The powdery 0.5Pt/pine-aqueous sample has shown higher activity ($T_{50} < 25$ °C) than the 0.5Pt/pine-freeze drying ($T_{50} = 48$ °C). This trend is in accordance with the results obtained above for the same catalysts in monolithic form. Both activities are in the order of our previously published Pt/SiC catalyst ($T_{50} = 34$ °C), tested in similar conditions than herein, and of Pt-substituted ceria based catalysts prepared by other authors and tested under 3% v/v H_2/air mixtures.[24,34]

4. Conclusions

Catalytic hydrogen combustion was studied under excess of oxygen in conditions that simulate the H_2 concentration of the exhaust gases from fuel cells (3–4% v/v H_2 in air). Bio-SiC based monoliths, prepared from different precursors (pine, sapele and MDF) have demonstrated to be efficient catalysts' supports. The obtained supports have shown different thermal and mechanical properties as well as different porosity according to their corresponding wood precursors. The election of the type of the bio-SiC based support will depend on the final application. Freeze drying has demonstrated to be the most efficient drying method to achieve homogeneous macroscopic and microscopic active phase distribution during the aqueous impregnation with CPA. This is very important to prevent hot spots.

The range of Pt loading herein tested (0.25–1.5 wt% Pt) was active enough to achieve almost 100% conversion at every flowrate at 3–4% H_2 concentration. Conversions are independent of active phase dispersion and particle size in our conditions. Hydrogen conversion (and also the temperature) increases with H_2 concentration and mixture flowrate under diffusional control. The results also point out to the idea that operation at high amounts of H_2, and consequently higher temperature, is beneficial to activity and that the catalyst is stable enough for long time operation even after long time air storage. However, for a real application in a fuel cell, the experiments should be scaled up to convert mixture flows up to 1000 times higher.

Temperatures profiles under diffusional control are consistent with the different thermal anisotropies measured in the bio-SiC supports. Pine derived bio-SiC monoliths have shown the highest anisotropy in thermal conductivity giving a maximum difference between the central and the side temperature of around 30 °C (T2 > T3). MDF monoliths have shown lower thermal anisotropy which was inverted respect to the one measured for pine, this producing higher temperatures on the side than in the center of the monolith (T2 < T3). Thermal anisotropy appears as a property of interest in this work which could be tuned by choosing the adequate wood precursor for the selected application.

Experiments in low conversion conditions reveal the importance of the cooling effect of the feeding mixture when considering the study of thermal management. Works are still in progress to improve homogeneity and dispersion of the active phase.

In sum, the use of bio-SiC based monoliths as catalysts supports for the CHC opens a new and interesting field of study. In particular we have explored the destruction of unreacted hydrogen at the exhaust of a fuel cell, but the results could be extended to other applications of these interesting reaction mainly considering anisotropy effects.

Acknowledgements

Notes and references

1 A. Züttel, A. Borgschulte and L. Schlapbach, in *"Hydrogen as a Future Energy Carrier"*, Wiley-VCH, 2008.
2 L. Schlapbach and A. Züttel, *Nature*, 2001, **414**, 353–358.
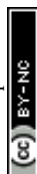
3 J. O. 'M. Bockris, *Int. J. Hydrogen Energy*, 2013, **38**, 2579–2588.

4 M. Al-Garni, *Int. J. Hydrogen Energy*, 1997, **22**, 383–387.

5 M. Haruta and H. Sano, *Int. J. Hydrogen Energy*, 1982, **7**, 737–740.

6 W. Choi, S. Kwon and H. D. Shin, *Int. J. Hydrogen Energy*, 2008, **33**, 2400–2408.

7 C. Zhang, J. Zhang and J. Ma, *Int. J. Hydrogen Energy*, 2012, **37**, 12941–12946.

8 P. A. Deshpande and G. Madras, *Phys. Chem. Chem. Phys.*, 2011, **13**, 708–718.

9 V. M. Shinde and G. Madras, *Catal. Today*, 2012, **198**, 270–279.

10 K. Ledjeff, *Int. J. Hydrogen Energy*, 1987, **12**, 361–367.

11 M. Haruta and H. Sano, *Int. J. Hydrogen Energy*, 1981, **6**, 601–608.

12 P. Marín, S. Ordóñez and F. V. Díez, *J. Chem. Technol. Biotechnol.*, 2012, **87**, 360–367.

13 P. Nguyen and C. Pham, *Appl. Catal., A*, 2011, **391**, 443–454.

14 A. R. de Arellano-López, J. Martínez-Fernández, P. González, C. Domínguez, V. Fernández-Quero and M. Singh, *Int. J. Appl. Ceram. Technol.*, 2004, **1**, 56–67.

15 P. Greil, T. Lifka and A. Kaindl, *J. Eur. Ceram. Soc.*, 1998, **18**, 1961–1973.

16 H. Sieber, C. Hoffmann, A. Kaindl and P. Greil, *Adv. Eng. Mater.*, 2000, **2**, 105–109.

17 M. Singh, J. Martínez-Fernández and A. R. de Arellano-López, *Curr. Opin. Solid State Mater. Sci.*, 2003, **7**, 247–254.

18 B. Alonso-Fariñas, M. Lupion, M. Rodriguez-Galan and J. Martinez-Fernández, *Fuel*, 2013, **114**, 120–127.

19 M. A. Bautista, J. Quispe Cancapa, J. Martinez Fernández, M. A. Rodríguez and M. Singh, *J. Eur. Ceram. Soc.*, 2011, **31**, 1325–1332.

20 C. R. Rambo, T. Andrade, T. Fey, H. Sieber, A. E. Martinelli and P. Greil, *J. Am. Ceram. Soc.*, 2008, **91**, 852–859.

21 A. Zampieri, H. Sieber, T. Selvam, G. T. P. Mabande, W. Schwieger, F. Scheffler, M. Scheffler and P. Greil, *Adv. Mater.*, 2005, **17**, 344–349.

22 Q. Wang, W. Z. Sun, G. Q. Jin, Y. Y. Wang and X. Y. Guo, *Appl. Catal., B*, 2008, **79**, 307–312.

23 T. L. Church, S. Fallani, J. Liu, M. Zhao and A. T. Harris, *Catal. Today*, 2012, **190**, 98–106.

24 A. Fernández, G. M. Arzac, U. F. Vogt, F. Hosoglu, A. Borgschulte, M. C. Jiménez de Haro, O. Montes and A. Züttel, *Appl. Catal., B*, 2016, **180**, 336–343.

25 C. Torres-Raya, D. Hernandez-Maldonado, J. Ramirez-Rico, C. Garcia-Gañan, A. R. de Arellano-Lopez and J. Martinez-Fernandez, *J. Mater. Res.*, 2008, **23**, 3247–3254.

26 G. Filardo, E. Kon, A. Tampieri, R. Cabezas-Rodríguez, A. Di Martino, M. Fini, G. Giavaresi, M. Lelli, J. Martínez-Fernández, L. Martini, J. Ramírez-Rico, F. Salamanna, M. Sandri, S. Sprio and M. Marcacci, *Tissue Eng., Part A*, 2014, **20**, 763–773.

27 F. M. Varela-Feria, J. Ramírez-Rico, A. R. de Arellano-López, J. Martínez-Fernández and M. Singh, *J. Mater. Sci.*, 2008, **43**, 933–941.

28 K. E. Pappacena, K. T. Faber, H. Wang and W. D. Porter, *J. Am. Ceram. Soc.*, 2007, **90**, 2855–2862.

29 M. A. Bautista, A. R. de Arellano-López, J. Martínez-Fernández, A. Bravo-León and J. M. López-Cepero, *Int. J. Refract. Met. Hard Mater.*, 2009, **27**, 431–437.

30 L. L. Snead, T. Nozawa, Y. Katoh, T. S Byun, S. Kondo and D. A. Petti, *J. Nucl. Mater.*, 2007, **371**, 329–377.

31 T. Vergunst, F. Kapteijn and J. A. Moulijn, *Appl. Catal., A*, 2001, **213**, 179–187.

32 T. A Nijhuis, A. E. W Beers, T. Vergunst, I. Hoek, F. Kaptejin and J. A. Moulin, *Catal. Rev.*, 2001, **43**(4), 345–380.

33 Y. Liu, I. Florea, O. Ersen, C. Pham-Huu and C. Meny, *Chem. Commun.*, 2015, **51**, 145–148.

34 P. A. Deshpande and G. Madras, *Appl. Catal., B*, 2010, **100**, 481–490.